CrossMark

Analysis of a severe dust storm and its impact on air quality conditions using WRF-Chem modeling, satellite imagery, and ground observations

Federico Karagulian [1,2] · Marouane Temimi [1] · Dawit Ghebreyesus [1] · Michael Weston [1] · Niranjan Kumar Kondapalli [1] · Vineeth Krishnan Valappil [1] · Amal Aldababesh [1] · Alexei Lyapustin [3] · Naira Chaouch [4] · Fatima Al Hammadi [5] · Aisha Al Abdooli [5]

Abstract

This study presents a comprehensive analysis of an extreme dust event recorded in the Arabian Peninsula and the United Arab Emirates (UAE) between 31 March and 3 April 2015. Simulations of the dust event with the Weather Research and Forecasting model coupled with the Chemistry module (WRF-Chem) were analyzed and verified using MSG-SEVIRI imagery and aerosol optical depth (AOD) from the recent 1-km Multi-Angle Implementation of Atmospheric Correction (MAIAC) algorithm for MODIS Terra/Aqua. Data from the National Centers for Atmospheric Prediction/National Center for Atmospheric Research (NCEP/NCAR) and the upper-air radiosonde observations were used to understand the synoptic of the event. In addition, the impact of the event on atmospheric and air quality conditions is investigated. The Air Quality Index (AQI) was calculated prior, during, and after the event to assess the degradation of air quality conditions. Simulated temperature, relative humidity, wind speed, and surface radiation were compared to observations at six monitoring stations in the UAE giving R^2 values of 0.84, 0.63, 0.60, and 0.84, respectively. From 1 to 2 April 2015, both observations and simulations showed an average drop in temperature from 33 to 26 °C and radiance reduction from about 950 to 520 Wm^{-2}. The AOD modeled by WRF-Chem showed a good correlation with Aerosol Robotic Network (AERONET) measurements in the UAE with R^2 of 0.83. The AQI over the UAE reached hazardous levels during the peak of the dust event before rapidly decreasing to moderate–good air quality levels. This work is the first attempt to demonstrate the potential of using WRF-Chem to estimate AQI over the UAE along with two satellite products (MODIS-MAIAC and MSG-SEVIRI) for dust detection and tracking.

Keywords Dust storm · Arabian Peninsula · WRF-Chem · Air Quality Index · Remote sensing · PM_{10} concentrations

---

✉ Marouane Temimi
marouane.temimi@ku.ac.ae

[1] Khalifa University of Science and Technology, Masdar Institute, P.O. Box 54224, Abu Dhabi, United Arab Emirates

[2] European Commission, Joint Research Centre (JRC), Energy, Transport and Climate Unit, Via Enrico Fermi 2749, 21027 Ispra, VA, Italy

[3] NASA Goddard Space Flight Center, code 613, Greenbelt, MD 20771, USA

[4] NOAA CREST Institute, The City College of the City University of New York, New York, NY, USA

[5] United Arab Emirate, Ministry of Climate Change & Environment, P.O. Box 1509, Dubai, United Arab Emirates

Introduction

Strong dust storms have adverse socioeconomic effects as they disrupt ground and air transportation systems (Kim et al. 2016). In addition, airborne particles emitted and transported during dust storms affect climate and weather systems by changing cloud microphysical properties (Seinfeld et al. 2016), atmospheric temperature profiles (Cheng et al. 2009), and surface irradiance (Liu et al. 2011). Moreover, airborne dust deteriorates air quality conditions and impacts human health due to an increase in the concentration of particulate matter (PM) (Zhang et al. 2016b) which can reach hazardous levels during extreme dust events (Kim and Chung 2008; Kim et al. 2012). Understanding the complex effects of such events, namely on atmospheric and air quality conditions and the interaction between them, is particularly important especially in dust-prone regions like the Arabian Peninsula.

The challenge facing the thorough analysis of dust storms and their impact on air quality and weather conditions in the Arabian Peninsula is the absence of dense air quality and weather monitoring networks in the region. Most of the published studies relied on satellite and numerical models to better understand the dynamics of events. Miller et al. (2008) focused on studying the haboobs over the UAE resulting from strong winds. They stated that haboob's contribution to the total dust production in the region might be as high as 30%. Another work by Notaro et al. (2013) that made use of trajectory analysis and MODIS satellite data to analyze a dust storm over Saudi Arabia found that higher aerosol optical depth (AOD) values are usually recorded during dust storms originating from the Rub' al Khali (Empty Quarter) and Iraqi deserts (NCM 2011).

Basha et al. (2015) used satellite data from MODIS, OMI, and CALIPSO to study an extreme dust event recorded between 18 through 22 March 2008, focusing on the impact on surface meteorological conditions and aerosol optical properties. The same dust event was also studied by Jish Prakash et al. (2015) who calculated the dust load generated by the storm and its deposition within the study domain. They stated that dust deposition may have a significant impact on the Red Sea marine ecosystem and possibly on the Gulf region as well (Al Azhar et al. 2016; Mezhoud et al. 2016). Both studies (Jish Prakash et al. 2015; Basha et al. 2015) showed that dust sources located in Iraq, Iran, and Kuwait, and the Arabian Peninsula Rub' al Khali desert contributed to the investigated extreme dust storm. However, their analyses focused on the dynamics of the events and their impacts on the meteorology without linking them to surface air quality conditions.

On the other hand, Beegum et al. (2018) studied the impact of extreme dust storms on air quality conditions and investigated a series of dust events using the CHIMERE model (Mailler et al. 2017) and satellite data over the Arabian Peninsula. They showed a significant socioeconomic impact of all studied dust events reflected in the degradation of visibility and air quality conditions. Radi et al. (2008) verified predictions of the Weather Research Forecasting-Chemistry (WRF-Chem) model against local observations of CO, NO_X, SO_2, and O_3 over the United Arab Emirates (UAE). They showed acceptable model performance as WRF-Chem–simulated AOD agreed well with observed AERONET AOD values. The same level of agreement was also noticed in the case of the other pollutants. Satellite observations from the Ozone Monitoring Instruments (OMI) were used over the Middle East to detect vertical column observations of nitrogen dioxide (NO_2), formaldehyde (HCHO), sulfur dioxide (SO_2), and glyoxal (CHOCHO) (Barkley et al. 2017). Findings showed that most of the above gaseous pollutants were underestimated when compared to the official emission inventories.

The goal of this study is to conduct a comprehensive analysis of an extreme dust event recorded between the 29 March and 3 April 2015 over the Arabian Peninsula which affected the UAE on 2 April 2015. The study addresses the event's impact on both the atmospheric and air quality conditions from the perspective of linking the magnitude of the storm to the degradation of air quality conditions. Furthermore, the interest is in investigating the dynamic of the extreme dust event and the persistency of its effect on air quality and meteorological conditions. This study integrates observations from satellite and ground observations along with simulations using WRF-Chem. In addition, the study intercompares information on dust extent from satellite observations and numerical models using WRF-Chem, analyzes their interconsistencies, and verifies them using ground-based observations. Eventually, the comparison of WRF-Chem outputs with satellite and station data allows for the assessment of the model and its parametrization over the UAE in the case of dust events, which has not been addressed in previous studies. Weather data obtained from the UAE National Center of Meteorology (NCM) network are used for the first time in the UAE to verify the model's performance and to assess the impact on atmospheric conditions. Concentrations of PM_{10} were inferred from the WRF-Chem simulation and satellite observations, and their consistency was evaluated. Furthermore, the Air Quality Index (AQI) was calculated using concentrations of simulated pollutants. The degradation of air quality conditions was assessed through the analysis of the levels of AQI, which was then discussed with respect to the country's air quality standards. This work aims to be a first attempt to estimate air quality levels using gaseous and particulate pollutants modeled from an air quality model such as the WRF-Chem. We have presented a case study using in a first attempt the WRF-Chem model over the region together with two satellite products to track and forecast dust over the Arabian Peninsula while analyzing the impact on air quality conditions.

Study domain and datasets

Study area

The study domain is shown in Fig. 1 a. Topography in the Arabian Peninsula gradually varies from flatlands on the eastern side of the peninsula to highlands on its western side. Desert land cover dominates the peninsula especially in its southeastern part where the Empty Quarter lies. In the UAE that is the focus of this study, topography is mostly flat, especially in the coastal and western parts of the country. The northeastern part of the UAE is dominated by the Al Hajar Mountain chain which stretches from the Omani coasts to the Strait of Hurmuz in the north, with peaks reaching an altitude
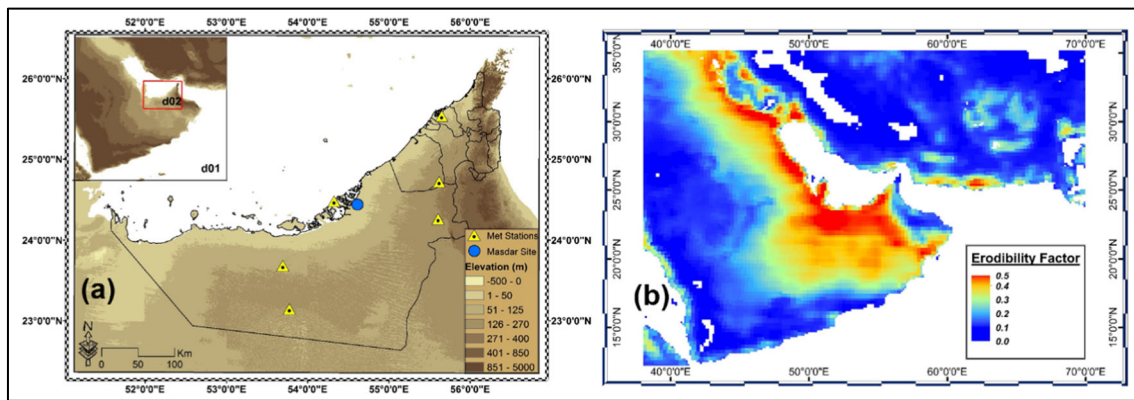
Fig. 1 **a** Location of the meteorological (triangles) monitoring sites in the UAE. Inset shows the main domain (d01) used for the WRF-Chem simulations. Terrain elevation over the Arabian Peninsula is shown as background of the map. Legend shows the elevation levels (in meters) over the study area. **b** Erodibility fraction map used in the WRF-Chem model from Ginoux et al. (2001)

of 1800 m (Fig. 1 a). Sand dunes are dominant in the western part of the UAE that is adjacent to the Empty Quarter. A rural land cover is prevailing in the western part of the country, with artificial urban cover, particularly in the emirates of Dubai and Abu Dhabi, with some dense shrub land to the east of Dubai (Wehbe et al. 2017; Wehbe et al. 2018). More details about the changing climate conditions in the UAE can be obtained from (Yousef et al. 2019).

Dust storms in the Arabian Gulf originate from dust sources coming from the Tigris and Euphrates River Valley regions of Iraq, East Syria, and Kuwait, and the low-lying flatlands in the east of the Arabian Peninsula, the Ad Dahna and the Rub' al Khali deserts in Saudi Arabia (Furman 2003; Shao et al. 2011). The spatial distribution of dust sources is in line with the spatial pattern of erodibility values (Ginoux et al. 2001) displayed in Fig. 1 b. The erodible fraction varies between 0 and 1 with the latter indicating high erodibility. The map in Fig. 1 b shows that, in most of the UAE, as well as the east side of the Arabian Peninsula, erodibility values are particularly high. Goudie and Middleton (2006) stated that eastern Syria, northern Jordan, and western Iraq are the sources of most of the "fine" dust particles (less than 50 mm in diameter) found in Arabian dust storms.

Precipitation over the Arabian Peninsula is low as the average annual precipitation is around 100 mm (Ghebreyesus et al. 2016; Ouarda et al. 2014; Wehbe et al. 2017). Rainfall events are usually short and sporadic. In the UAE, vegetation cover in the region is mostly limited to landscaping in urban areas or to farming activities. Despite low precipitation, fog is frequent especially during the months of November, December, and January. Fog results from strong temperature inversion in the desert which causes dew formation at the soil surface at night and early morning (Aldababseh and Temimi 2017; Chaouch et al. 2017; Weston et al. 2018) and may suppress dust emission temporarily (NCM 2011). When fog burns off just after sunrise, soil moisture decreases rapidly restoring soil erodibility.

The winter season in the Arabian Peninsula is characterized by cold air carried into the region by quasi-stationary Siberian High pressure in the east, generating strong northwest winds with speeds up to 15–20 m s^{-1} (Crook 2009). The topography of the region plays a major role in strengthening the wind with the high terrain along the Iranian Coast and along the west coast of Saudi Arabia producing a "wind funnel" through the region (Giannakopoulou and Toumi 2012). This wind is usually referred to as shamal wind which is specific to the region. Shamal winds blow in the Arabian Gulf during the summer (June to August) and the winter (November to March). While the summer shamal blows continuously, the winter shamals are short, from 24 h to 3–4 days (Perrone 1979; Prospero et al. 2002). The winter shamal is associated with mid-latitude disturbances that progress from west to east and occurs following a cold frontal passage with consequent reduction of temperature. Winter shamal winds in the Arabian Gulf region are stronger (Michael Reynolds 1993) as they reach up to 25 m s^{-1} and generate a large amount of airborne dust (Wilkerson 1991).

Datasets

Weather data

The National Centers for Atmospheric Prediction/National Center for Atmospheric Research (NCEP/NCAR) reanalysis data (Kalnay et al. 1996) were used to analyze the synoptic conditions of the dust event from 31 March to 3 April 2015. We used NCEP/NCAR temperature, winds, sea level pressure, and geopotential height at a resolution of 0.5° × 0.67° at 00, 06, 12, and 18 UTC.

Atmospheric vertical structure was analyzed using radiosonde (RS) data at the Abu Dhabi International Airport (24.4° N 54.6° E) (http://weather.uwyo.edu/upperair/sounding.html). The RS provides profiles of pressure, temperature, water vapor, and wind speed and direction. The RS data were used

to detect temperature inversions, atmospheric instability, and the planetary boundary layer (PBL) extension over the Abu Dhabi area. Ground measurements of meteorological parameters including temperature, relative humidity, wind speed, and solar radiation were obtained for six monitoring stations across the country (Fig. 1 a) from the UAE National Centre of Meteorology (NCM).

Dust flag

The dust storm was detected and tracked over the Arabian Peninsula using satellite data from the Spinning Enhanced Visible and Infrared Imager (SEVIRI). This sensor is located on the MSG (Meteosat Second Generation) series of satellites operated by the European Organization for the Exploitation of Meteorological Satellites (EUMETSAT). SEVIRI is a geostationary sensor which provides images every 15 min at a resolution of 3 km with 1-km sampling distance at nadir (Schmetz et al. 2002). For our study, we used SEVIRI dust masks (Dust Flags, SDF) (Banks and Brindley 2013; MétéoFrance 2011) which were successfully tested and verified over the Middle East and North Africa regions.

AOD data

The Moderate Resolution Imaging Spectroradiometer (MODIS) on Terra and Aqua satellites provides global aerosol properties over land and ocean. Over bright deserts, the AOD is available from the Deep Blue (Hsu et al. 2013) and the recently released Multi-Angle Implementation of Atmospheric Correction (MAIAC) algorithm (Lyapustin et al. 2018). Both algorithms provide AOD at 550 nm, though MAIAC product is at 1-km resolution and gridded while the Deep Blue AOD is reported at 10-km nadir resolution and in swath format. Due to UAE's sub-tropical latitude, Terra and Aqua overpass time over the UAE is ~ 10:30 am and 1:30 pm (local time), respectively. The Aerosol Robotic Network (AERONET) (Holben et al. 1998) provides a globally distributed ground-based observations of spectral AOD and derived optical properties. This work used cloud-screened Level 1.5 aerosol data for sun photometer located at Masdar City in Abu Dhabi (UAE) (Fig. 1) to validate MAIAC AOD as well as the WRF-Chem numerical simulations.

Methods

WRF-Chem model

The Advanced Weather Research and Forecasting (WRF-ARW v3.8.1) model with the chemistry/aerosol module (WRF-Chem) was used to simulate emissions of aerosols and gases, their transport, and chemical and microphysical transformations of trace gases and aerosols (Grell et al. 2005; Peckham et al. 2015). The configuration of WRF-Chem is shown in Table 1. WRF-Chem simulations were carried out over two nested domains (d01 and d02) with a spatial resolution of 12 km and 4 km, respectively. The inset map in Fig. 1 a shows WRF-Chem (d01) domain which extends over a large area of the Arabian Peninsula, allowing the inclusion of dust sources in Iraq, Kuwait, and Saudi Arabia.

The model was initiated using meteorological data (GFS 0.5 degree) from the National Centers for Environmental Prediction (NCEP) at 00 UTC on 29 March 2015 and was forced by the same dataset every 6 h. WRF-Chem surface variables were extracted at the altitude level of 10 m for the wind speed and wind direction, 2 m for the temperature, relative humidity, and barometric pressure. AOD was obtained from WRF-Chem by vertical integration (from the ground to the top of the domain, i.e., 20 km) of the aerosol extinction coefficient at 550 nm, which was obtained as the direct output of the WRF-Chem. The WRF-Chem model was configured with emission data from EDGAR-HTAP at a resolution of $0.1 \times 0.1°$ (Greet et al. 2012). For dust emissions, we used the erodibility map from Ginoux et al. (2001) (see Fig. 1 b). The calculation of dust emission in the atmosphere was performed using the Goddard global ozone chemistry aerosol radiation and transport (GOCART) emission scheme (Ginoux et al. 2001). The GOCART emission scheme was coupled with the regional acid deposition model 2 (RADM2), the modal aerosol dynamic model for Europe (MADE), and the secondary organic aerosol model (SORGAM) (Ackermann et al. 1998). The Goddard scheme for shortwave (Mlawer et al. 1997) and the Rapid Radiative Transfer Model (RRTM) for longwave (Chou and Suarez 1994) were used for the aerosol direct radiative effect.

HYSPLIT back trajectories

The location of Abu Dhabi International Airport (24.4° N 54.6° E) was chosen as a receptor point to compute back trajectory simulations at two altitudes of 500 and 1500 m for a period of 72 h from the Hybrid Single Particle Lagrangian Integrated Trajectory (HYSPLIT) model (Stein et al. 2015). Back trajectory analysis allows for the understanding of the track of dust plume at different altitudes but not necessarily the determination of their sources. The goal here is to understand the transport process during the dust event and use it to verify the trajectories inferred from satellite and model outputs.

The Air Quality Index determination

The AQI is a number that ranks air quality conditions based on criteria associated with the effect that concentrations of different pollutants might have on human health. The AQI is, therefore, a number associated to a rank that is translated into a

Table 1 WRF-Chem model setup parameters

Domains	Parent domain, 12 km ($249 \times 209 \times 44$)	
	Nest domain, 4 km ($249 \times 262 \times 44$)	
Vertical levels	44	
Boundary conditions	NCEP-GFS	
Time step	60 s	
Output intervals	60 min	
Simulation period	31 March–3 April 2015	
Physics schemes	sf_surface_physics = 2	Noah land surface model (Chen and Dudhia 2001)
	bl_pbl_physics = 1	YSU (Hong et al. 2006)
	sf_sfclay_physics = 1	MM5 (Monin and Obukhov 1954)
	mp_physics = 2	(Lin et al. 1983)
	ra_sw_physics = 2	Goddard shortwave (Mlawer et al. 1997)
	ra_lw_physics = 1	RRTM scheme (Chou and Suarez 1994)
	aer_op_opt = 1	MIE theory
Chemistry scheme	chem_opt = 300	GOCART SIMPLE (Paul Ginoux et al. 2001)
Emissions inventory	emiss_opt = 3	MADE/SORGAM (Shell and Somerville 2007)
Dust scheme	dust_opt = 1	GOCART (used fractional erosion data map)

"category" of risk on human health. Such values are usually reported by government agencies to the public as an indication of the "healthiness" of the air. AQIs have been calculated from concentrations of O_3 (Ozone), $PM_{2.5}$, PM_{10}, CO (carbon monoxide), NO_2 (nitrogen dioxide), and SO_2 (sulfur dioxide) simulated from 29 March to 4 April 2015. For the calculation of the AQI, in addition to the US-EPA methodology (EPA 2006), we have used specific AQI breakpoints for the pollutants O_3 and PM_{10} according to the Air Quality Regulation enforced in the UAE (Decree 2006). AQI criteria in the UAE differ from US EPA criteria mainly for setting the first category (good 0–50) that is set to the threshold concentration level of 150.4 μg/m^3, 100.4 μg/m^3, 75.4 μg/m^3, 10.4 mg/m^3, and 20.4 μg/m^3 for PM_{10}, O_3, NO_2, CO, and SO_2, respectively. In the absence of a $PM_{2.5}$ limit value in the UAE, we have used the limit value of 12 μg/m^3 according to the EPA regulations. The AQI was then calculated according to the following equation:

$$AQI = \frac{AQI_{high} - AQI_{low}}{C_{high} - C_{low}} (C - C_{low}) + AQI_{low} \qquad (1)$$

where AQI_{high} is the AQI, C is the concentration of the pollutant, C_{low} is the cutoff point for 24-h average concentration of PM_{10}, $PM_{2.5}$, NO_2, SO_2, and, for 8-h average concentration of O_3 and CO. C_{low} is lower or equal to C, C_{high} is the 24-h average pollutant concentration that is higher or equal to C, and AQI_{low} is the AQI corresponding to C_{low}. There are six AQI breakpoint categories associated with health effects: good, 0–50 (no health risks); moderate, 51–100 (moderate health effects); unhealthy, 101–150 for sensitive groups (possible health risks for newborns, young children, pregnant

women, and elderly); unhealthy, 151–200 (everyone might have health effects); 201–300, very unhealthy (everyone might have several health effects); and hazardous, 301–500 (emergency conditions).

Results

Synoptic conditions and simulation of the dust event

The synoptic conditions during the evolution of the dust storm are assessed based on the National Centers for Atmospheric Prediction/National Center for Atmospheric Research (NCEP/NCAR) reanalysis data. Figure 2 a shows the upper tropospheric zonal winds between 31 March and 03 April 2015. The two jet streams viz. Subtropical (between 25 and 40 N and 10 and 60 E) and Polar (45 and 60 N and 0 and 20 E) are noticeable and are clearly separated from each other on 31 March 2015. On 01 April 2015, the Polar jet, which is more dynamical than the Subtropical jet, is more advanced to low latitudes. The two jet streams converge into a single jet maximum over the Eastern Mediterranean region on 02 April 2015, and the merging weakens on 03 April 2018. The convergence of the two jet streams has a strong influence on the surface below the northeastern part of the upper-level maximum winds (01 April 2018), especially in the presence of fronts (Hamidi et al. 2013; Middleton 1986). This is depicted clearly in Fig. 2 b, where we show the geopotential heights (contours) at 500 hPa overlaid with the lower tropospheric wind vectors (850 surface). A mid-tropospheric trough is noticeable over the Eastern Mediterranean region on 31 March 2018 that is moving eastward on the following days.
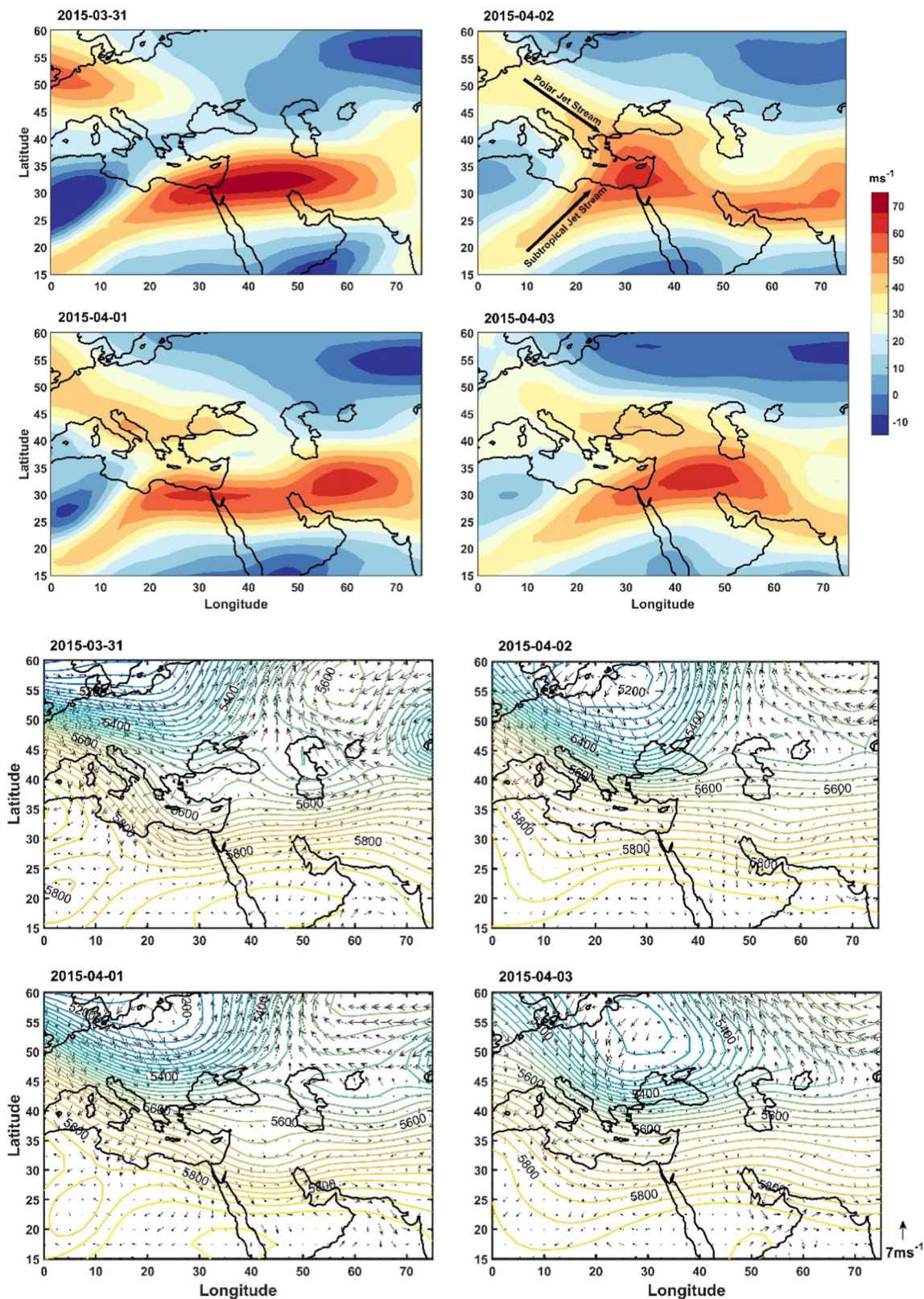
Fig. 2 **a** The daily upper tropospheric (200 hPa) zonal winds (m/s) derived from the NCEP/NCAR reanalysis data between 31 March and 3 April 2015. **b** Contours indicate the daily mid-tropospheric (500 hPa) geopotential heights (m) overlaid with 850 hPa-sfc wind vectors (m/s) derived from the NCEP/NCAR reanalysis data between 31 March and 3 April 2015. The geopotential contours are plotted from 4800 to 5800 m with an interval of 200 m. The wind vectors are scaled with a reference magnitude of 7 ms^{-1}. **c** Same as **a** but for the daily sea level pressure (hPa) between 31 March and 3 April 2015 derived from the NCEP/NCAR reanalysis data
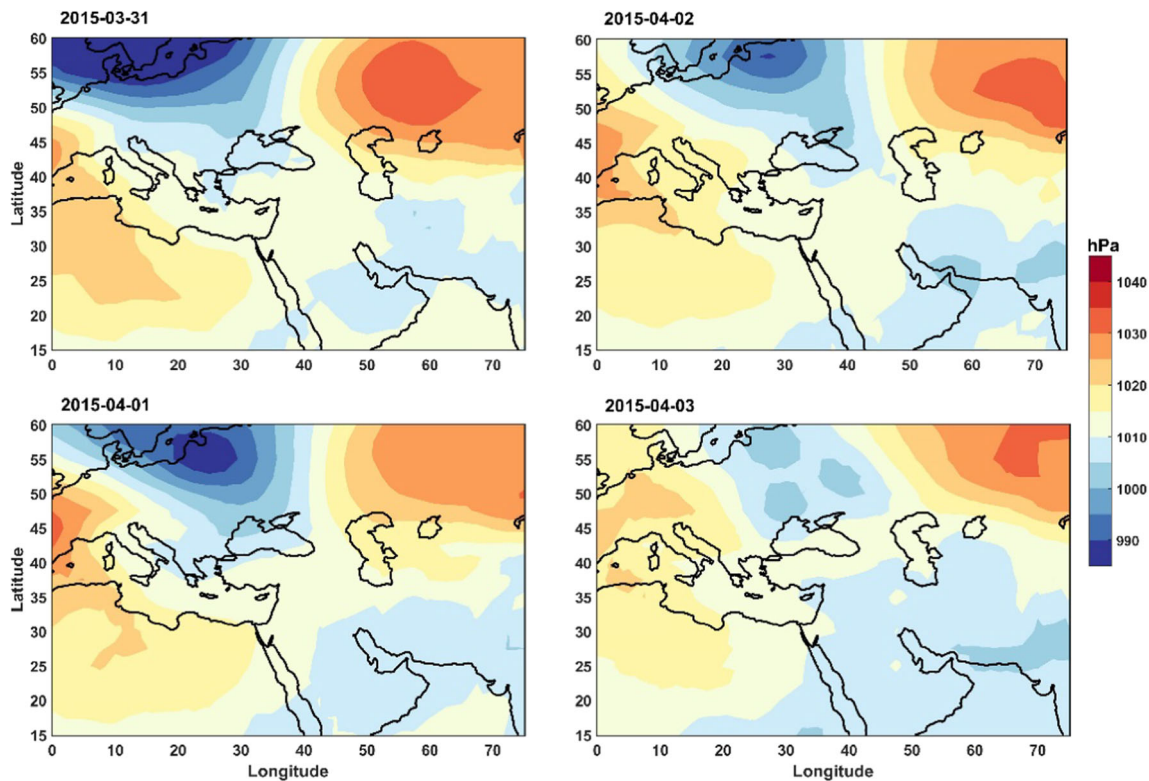
Fig. 2 continued

Figure 2 b also depicts eastward moving Polar trough that intrudes more southward on 01 April 2018. The strong southward wind flow on 01 April 2018 (Fig. 2 b) toward the Arabian Peninsula is also clearly discernable. This also supports that the convergence of the two jet streams has a strong influence on the surface winds. Figure 2 c shows the sea level pressure during the evolution of the dust storm. The troughs and ridges at polar latitudes shown in Fig. 2 b and c are part of the synoptic scale wave disturbances associated with convergence and divergence in the presence of the jet stream. On 01 April 2018, an intense low pressure area is also seen over the eastern part of the UAE and adjoining Arabian Gulf. The low pressure enhances the eastward surface winds creating a cyclonic circulation over the UAE region on 01 April 2018 (Fig. 2 b). Hence, the synoptic conditions, especially the convergence of the jet streams, create favorable conditions for the generation of the dust storm on 01 April 2018.

In Fig. 3, we show the effect of the large-scale dynamics on the local scale using the RS measurements. For instance, the RS data at the Abu Dhabi airport show a progressive decrease of air temperature on March 31 indicating a normal temperature profile (Fig. 3). However, on April 1, it was possible to observe a decrease in the surface temperature compared to the previous day. In addition, a low-level temperature inversion at ∼ 2 km was also observed (Fig. 3). The inversion is developed due to the cold air that is blowing from higher latitudes as depicted in Fig. 2 b on 01 April 2018. On

April 2, the drop of the surface temperature was observed to be constant indicating unstable conditions and a possible deeper inversion and growth of the boundary layer over the Abu Dhabi Airport. A deeper inversion is an indicator of unstable conditions and could be the result of competing effects related to the meteorology but also to the warming effect of the dust in the atmosphere through scattering and absorption.

The low-level inversion observed on April 1 was associated with wind gradient triggering the formation of the dust storm over Abu Dhabi on April 2. Figure 3 shows a noticeable change in wind speed and direction around a 1.5-km altitude that is similar to the height of the inversion on April 1. According to RS sounding observations, the wind speed was higher (∼ 8 ms^{-1}) at the surface and up to a 3-km altitude on April 2 and 3. However, on April 2, unlike that on April 3, wind speed increased significantly starting from a 3-km altitude and reaching up to 28 ms^{-1}, which was a clear indicator of unstable conditions. On April 1, the vertical profile of the wind direction showed an inversion at around a 1-km height with consequent decrease of the wind speed down to ∼ 5 ms^{-1}. However, on April 2, the RS profiles showed a significant decrease of air temperature down to ∼ 26 °C with wind speed up to 13–14 ms^{-1}. Moreover, on April 1, the RS water mixing showed a significant gradient at an approximately 2.5-km altitude which was in agreement with the inversion layer observed for the temperature profile (Fig. 3).

Fig. 3 Radiosonde profiles of temperature, wind direction, mixing ratio, and wind speed at the Abu Dhabi International Airport (AUH). Data are referred to 12 UTC from March 31 to April 1, 2015
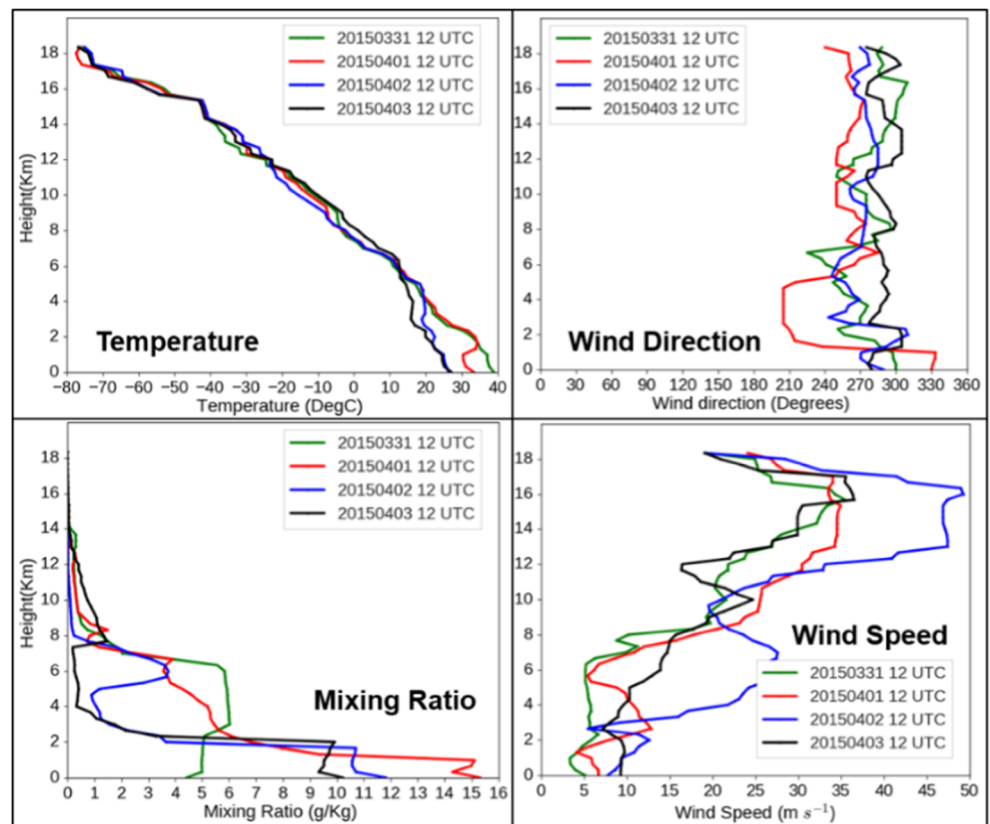
The analysis of the synoptic conditions and RS observations was supported by the analysis of surface observation from six meteorological stations. Surface observations were also used to assess the performance of WRF-Chem simulation through the comparison between ground observations and simulations which are shown in Fig. 4. Simulated time series of temperature, wind speed, relative humidity, and radiation were obtained from WRF-Chem simulations (domain d02, Fig. 1 a) at the selected six sites in the UAE. Summary statistics about the comparison between measured and simulated meteorological variables are reported in Table 2. The wide impact of the dust storm can be clearly observed in the time series shown in Fig. 4 where temperature, wind speed, relative humidity, and radiation mainly followed the same trend over the duration of the dust event at different locations in the UAE. A good agreement was observed between simulated and measured meteorological parameters. Results indicated that between 1 and 2 April 2015, when the dust event was recorded, surface temperature dropped, on average, from 33 to 26 °C (Fig. 4 a). The drop in surface temperature indicated the surface cooling effect of the dust plume which impacted all stations because of the widespread nature of the event. This temperature drop persisted on April 3 and April 4, maintaining an average temperature around 26 °C. The WRF-Chem model simulated reasonably well the drop in temperature as a result of the dust event especially in post-event conditions, between

April 3 and April 4. On April 2, during the peak time of the dust event, all the meteorological stations showed an overestimation of surface temperature compared to observations which could be related to an underestimation of aerosol optical depth right before or during the dust event. The metric reported in Table 2 summarizes the level of agreement (R^2) and accuracy (slope) of the comparison between ground-based measurements and modeled data. Overall, radiation and temperature showed a good level of agreement and accuracy when evaluated over the locations of the monitoring stations. However, while relative humidity (RH) and wind speed (WS) showed good accuracy between measurements and modeled data, their agreement was relatively low. On the other hand, a good agreement was observed between observed and modeled AOD.

The analysis of relative humidity (RH) showed, on average, a drop from 53 to 46% on April 2 with respect to pre-dust conditions (Fig. 4 b). Almost all stations, except at the Abu Dhabi Airport, showed an increase in RH that started toward the end of April 2 and continued on April 3 after the dust event with a peak of around 80%. A higher RH on April 3 could have contributed to the reduction of dust concentration. On the other hand, the lower RH observed from April 1 until the afternoon of April 2 fostered dust transport and emission because of the prevailing dry conditions. This was in agreement with the high mixing

Fig. 4 **a** Time series of measured (red line) and WRF-Chem simulated temperature (blue line) during the dust event on April 2015 at selected locations in the UAE; **b** same as **a** for relative humidity; **c** same as **a** for wind speed; **d** same as **a** for SW radiation
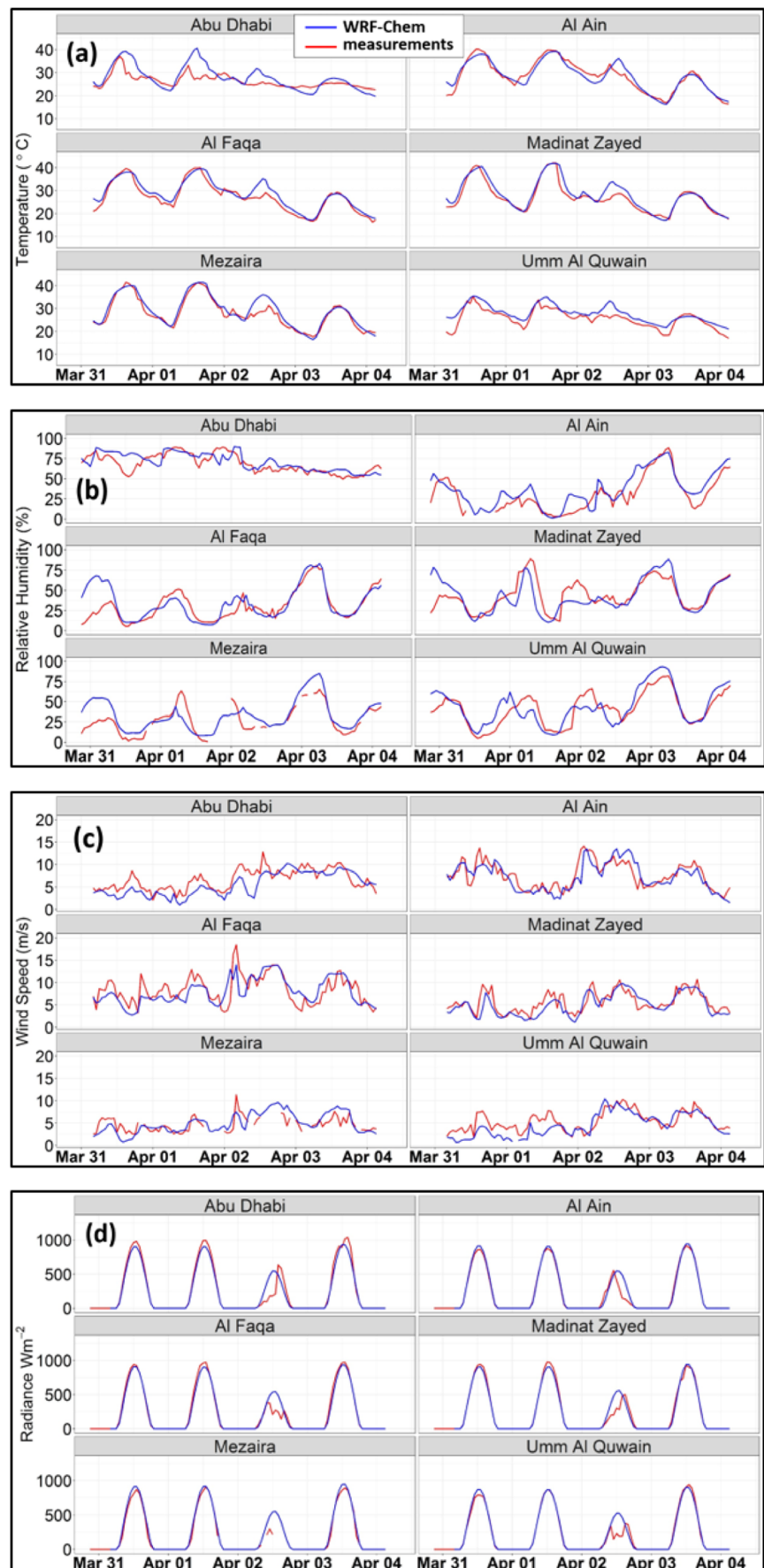
Table 2 Summary statistics from the comparison between measured and WRF-Chem modeled temperature, relative humidity, wind speed, radiation, and AOD (AERONET) as shown in Fig. 7

Measurements vs. WRF-Chem comparison					
	Intercept (±SE)	Slope (±SE)	R^2	Residual SE	Bias*
Temperature (°C)	2.0 ± 0.47	0.89 ± 0.02	0.84	2.29	5%
Relative humidity (%)	3.12 ± 1.1	0.81 ± 0.22	0.63	14.8	9%
Wind speed (ms^{-1})	0.67 ± 0.16	0.73 ± 0.25	0.60	1.74	10%
Radiation (Wm^{-2})	0.35 ± 0.20	0.92 ± 0.25	0.84	52.0	5%
AOD (AERONET vs. WRF-Chem)	0.27 ± 0.06	0.66 ± 0.07	0.83	0.23	7%

*Bias is referred to the percentage difference between measured and simulated data

ratio RS values reported on April 1 at 12 UTC at the Abu Dhabi International Airport which should have led to high RH especially with the continued decline in temperature. Indeed, RH was the highest on the evening of April 2 until the early morning of April 3.

The presence of a high dust concentration indirectly affected the radiative budget by the combined effect of absorption and scattering (Ackerman and Chung 1992; Cautenet et al. 1992; Markowicz et al. 2003). The presence of dust directly affected the amount of solar radiation reaching the surface which could be seen in the shortwave radiation measurements reported in Fig. 4 d. In the case of significant increase of dust density and aerosol optical depth, a near shutdown of short-wave radiation may occur reproducing nighttime-like conditions at the surface where longwave radiation prevails. In the case of the investigated event, a significant decrease in short-wave radiation was observed from about 950 to 520 Wm^{-2}. This decrease corroborates the surface cooling reflected in the temperature values in Fig. 4 a. WRF-Chem simulated the variability of SW radiation reasonably well with a slight overestimation on the morning of April 2 as the dust storms started developing in the UAE. The overestimation of surface SW radiation is concurrent with the surface temperature overestimation reported at all stations. It is expected that the presence of dust affects longwave radiation as well which should trigger a warming in the atmosphere. Such measurements of longwave radiation are not available to demonstrate it. However, the surface cooling effect of dust over other areas was reported in other studies (Haywood and Boucher 2000; Miller et al. 2008; Schell et al. 2001; Tegen and Lacis 1996). The magnitude of the cooling and decline in the radiation reflected in the observed values are relevant to report in the specific context of this study.

Satellite remote sensing of the dust event

Snapshots of AOD satellite images illustrating the dynamic of the dust event across the Arabian Peninsula are shown in Online Resource 1. According to the used data products, namely MAIAC and Deep Blue AOD, it could be noticed that, on 1 April 2015, a massive amount of dust was blowing out of

the northwest portion of the Arabian Peninsula and moving southward across the Arabian Peninsula. On April 2, the dust curved toward the UAE crossing the Arabian Gulf toward Iran after sweeping across Saudi Arabia's Rub' al Khali, or Empty Quarter. Finally, on April 3, the dust plume moved further southward across Yemen and Oman clearing the UAE region, further moving toward the Sea of Oman where it started dissipating.

A good agreement was obtained between satellite images processed with the Deep Blue algorithm (here called MODIS) and the MAIAC algorithm. The agreement was less significant on April 1 where MAIAC data showed lower AOD values over the UAE compared to MODIS observations (Online Resource 1(a)) which concurred with the SEVIRI dust flags and the WRF-Chem model which did not show any considerable amount of dust over the UAE, on 1 April (Fig. 5). However, the comparison between dust mask obtained from SEVIRI and MAIAC (AOD > 0.75) revealed the same pattern with MAIAC observations missing some features in the Omani region. On April 2, while the SEVIRI dust flag seems to properly delineate the extent of the dust plume, it is clear that an area in the center of the plume corresponding to the highest AOD values in MAIAC (Fig. 5 a) was not flagged as dust. This could be attributed to the thresholds used in the SEVIRI dust flag algorithm which might need to be adjusted over the Arabian Peninsula as the product was developed for the entire Middle East and North Africa (MENA) region. Indeed, the dust flag has two sets of thresholds corresponding to fine and coarse particle detection. The size of the particles involved in the studied dust storm in the non-flagged area, and their optical and radiative properties, could be inappropriate for the pre-defined thresholds in the dust flag decision tree.

AOD observations from MAIAC recorded the highest value (~ 4) over the UAE and Southern Saudi Arabia on April 2: that was the day when the dust event transformed into a dust storm over the UAE (Online Resource 1(a)). WRF-Chem simulations of AOD showed patterns similar to satellite observations but with evident underestimation of the dust over Southern Saudi Arabia on April 2 and 3 (Fig. 5 c). The underestimation of the spatial distribution of AOD observed from the WRF-Chem could be associated to the overestimation of
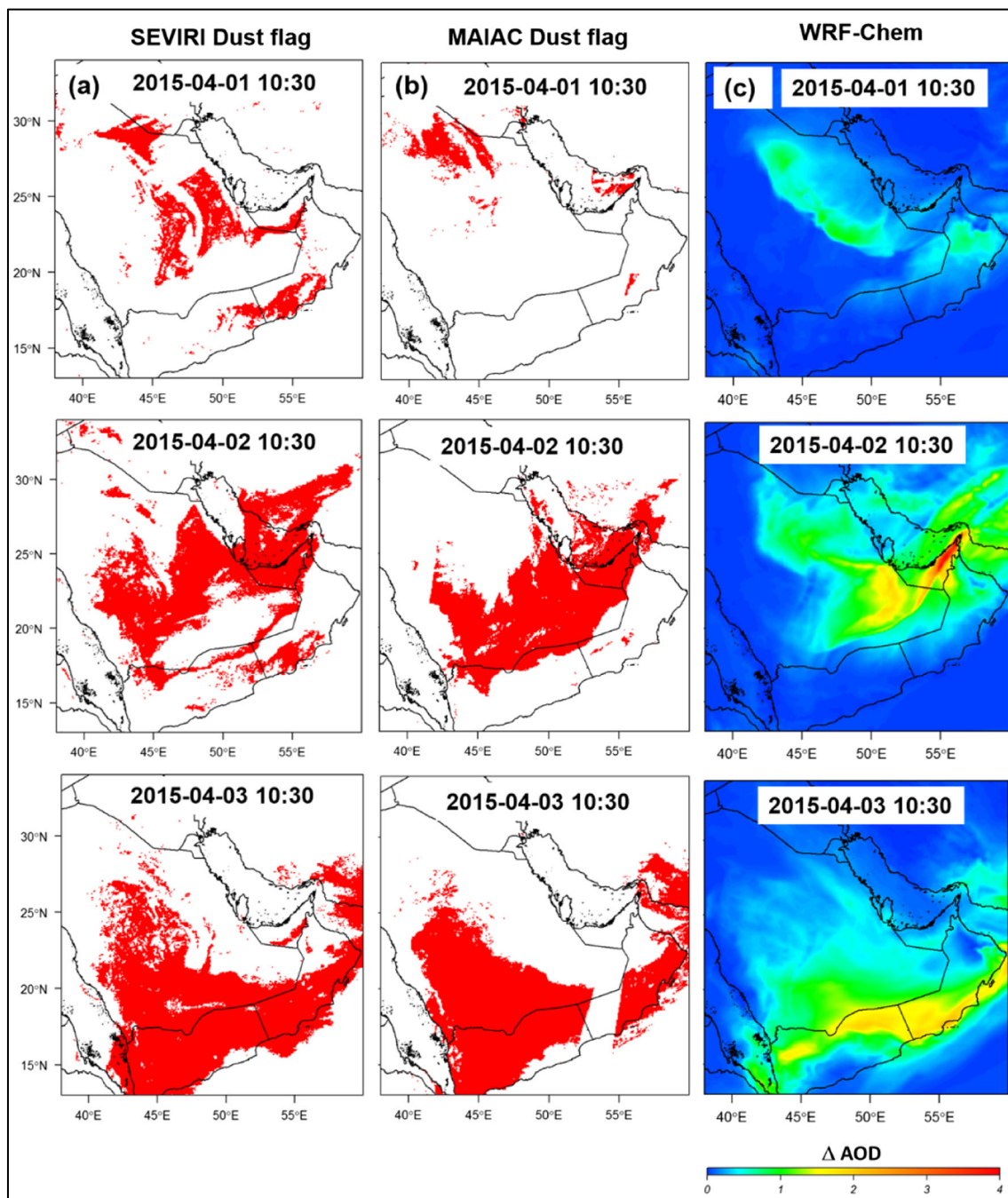
Fig. 5 **a** SEVIRI dust masks estimated with the SDF algorithm from Banks et al. (MétéoFrance 2011; Banks and Brindley 2013); **b** dust mask obtained from MAIAC-AOD > 0.75; **c** WRF-Chem simulations. Data are at 1-km spatial resolution

surface radiation reported above in Fig. 4 and which led to an overestimation of surface temperature. Additionally, an inaccurate wind threshold velocity in the WRF-Chem model has possibly impacted the simulation of dust emission and transport (Cremades et al. 2017; ElTahan et al. 2017; Nabavi et al. 2017; Rizza et al. 2018; Su and Fung) and therefore AOD values.

Maps of AOD differences (a) MAIAC observations and SEVIRI, (b) MAIAC and WRF-Chem model, and (c)

MODIS and MAIAC (Online Resource 2) showed better capability of MAIAC algorithm to detect dust over Saudi Arabia's Rub' al Khali as well as over the southwestern part of the Arabian Peninsula. MAIAC data showed wider spatial coverage in the detection of dust over the studied region. In addition, MAIAC data reported higher AOD values compared to MODIS observations and WRF-Chem simulations.

HYSPLIT back trajectories, simulated at the receptor location of the Abu Dhabi International Airport on April 1,

Fig. 6 72-h HYSPLIT back trajectories calculated for the dust event that occurred on 1 April 2015 over the UAE. The receptor point of the trajectories has been chosen at the Abu Dhabi Airport. Colors represent the 24 h of the days at intervals of 4 h each. The length of each trajectory is referred to the 72-h path to reach the receptor point. Time is at UTC + 04:00
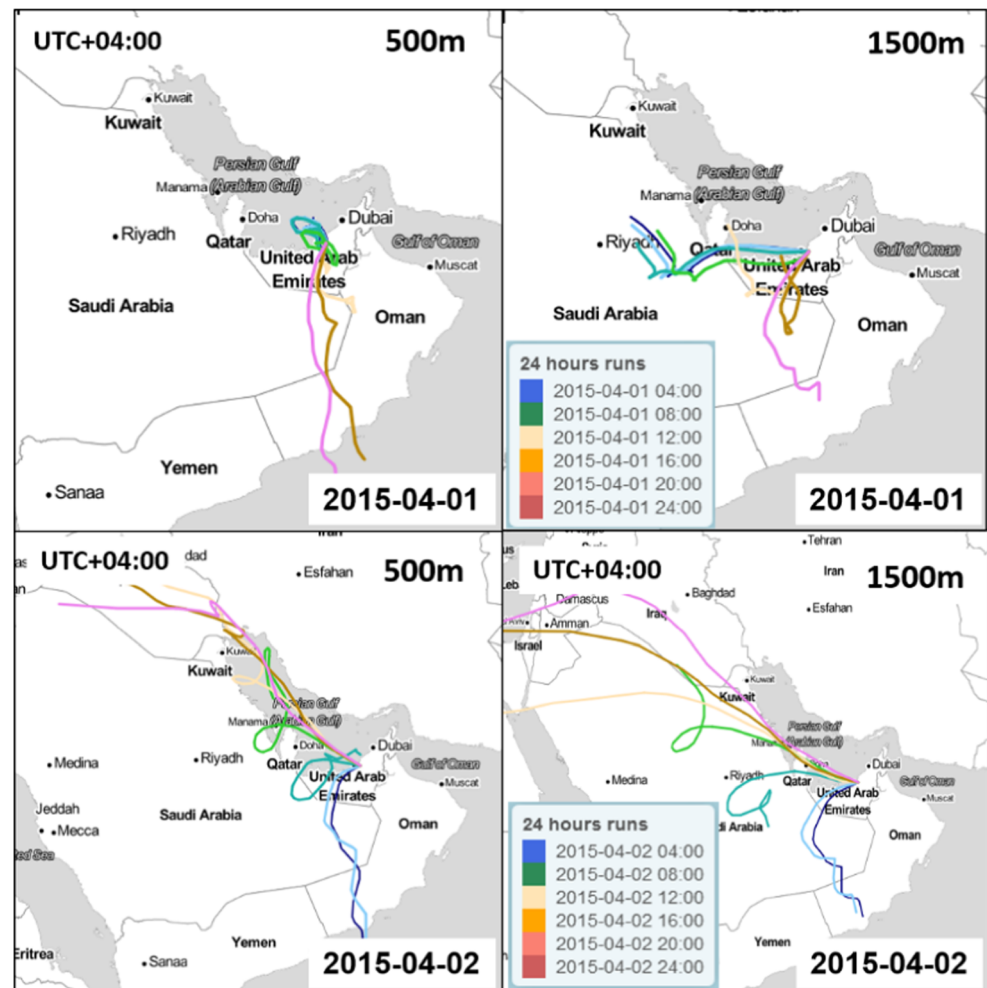
showed wind flows coming from Oman at a 500-m altitude in the boundary layer (Fig. 6). On the other hand, at a higher altitude of 1500 m, winds were also coming from Northern Saudi Arabia. On April 2, when the dust event impacted the UAE, one wind flow originated from Oman in the morning, whereas another wind flow originated from Iraq later in the day. The inferred back trajectories are in agreement with satellite snapshots of the dust plume. The persistent low-level wind on April 2 along the eastern side of Saudi Arabia coincided with the region of high erodibility factor in the Peninsula (Fig. 1 b) which fostered the emission of more dust toward the UAE. The wind was blowing from northwest at a speed of ~ 15 ms^{-1}.

Comparison of AOD from WRF-Chem, MODIS, and Masdar AERONET

AOD values obtained from WRF-Chem simulation (nested domain (d02)) and MODIS-MAIAC (Aqua and Terra) were verified using AERONET measurements at Masdar station in

the UAE (Fig. 7). Daily estimates of AOD from MAIAC data were used in the comparison. Figure 7 shows the hourly resolved time series of AOD at 550 nm for the WRF-Chem simulation (black line), the AOD MODIS-MAIAC retrievals (blue line), and the corresponding AERONET measurements at the Masdar station (dashed line). The WRF-Chem simulation showed the highest peak of AOD at ~ 2.2 on 2 April 2015 at ~ 12:30 pm (local time). On the other hand, AERONET observation and MODIS-MAIAC showed AOD peaks reaching values of 1.9 and 1.4 at ~ 1:30 pm, respectively. On the other hand, WRF-Chem simulations underestimated AOD from March 29 to April 1 when compared with AERONET and MAIAC estimates. The inaccuracy of WRF-Chem during the first days of the event could be attributed to the initialization of the model and the lack of the appropriate boundary forcing. Summary statistics about the comparison between measured and simulated AOD intensity is reported in Table 2 and in Fig. 7. Results showed that, overall, the correlation (R^2) between AERONET and modeled AOD was 0.82 with an overall bias as low as 7%.
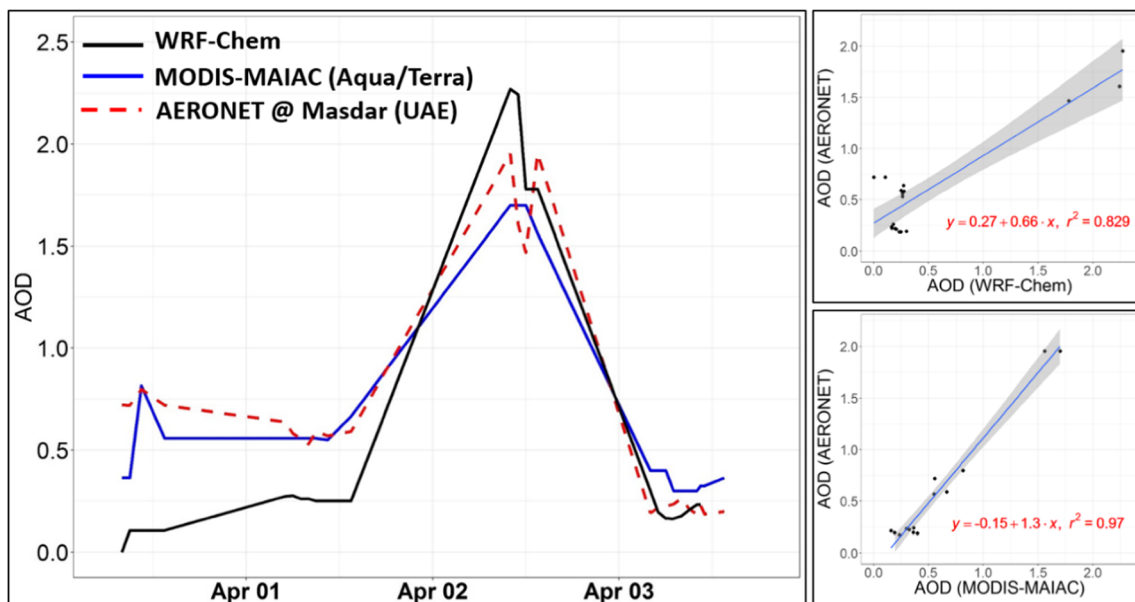
Fig. 7 Comparison of AERONET AOD (550 nm) observations at Masdar Institute (Abu Dhabi-UAE) with MODIS-MAIAC (Aqua and Terra) data and WRF-Chem simulations. Gray shades in the fit plots indicate a pointwise 95% confidence interval on the fitted values

Impact of the dust event on air quality conditions

The degradation of air quality conditions due to the dust event was analyzed in and around the UAE where concentrations and therefore AQI were calculated according to the country's thresholds as explained in the section "The Air Quality Index determination." Simulated PM_{10} concentrations at a spatial resolution of 4 km over the UAE are shown in Fig. 8. On 1 April 2015, a higher concentration of PM_{10} in the order of 750 μg/m^3 could be noticed in the Empty Quarter in Saudi Arabia and the eastern part of the domain on the borders between the UAE, Oman, and Saudi Arabia as result of the northwesterly strong wind in Saudi Arabia and southwesterly wind in Oman. It is worth noting that the predominant higher values of PM_{10} concentrations on April 1 seem to drop to ~200 μg/m^3 along the Hajar Mountain chain in UAE and Oman (Fig. 8). On April 2, the spatial distribution of the simulated PM_{10} clearly showed that the whole region was impacted by the event as the concentrations were above 1000 μg/m^3 in the UAE and most of the

study domain. The highest concentrations above 1500 μg/m^3 were obtained along the west coast of the UAE around large cities like Abu Dhabi and Dubai. This high concentration is close to the peak concentration of 1600 μg/m^3 that was reported at the Abu Dhabi Airport site by Basha et al. (2015) during another extreme dust event that occurred between 17 and 22 March 2012 over the UAE. In their study, they used simulations from The Earth Sciences Department from the Barcelona Supercomputing Center (BSC) using the Dust Regional Atmospheric Model (DREAM) called BSC-DREAM8b v2.0. The impact of the Hajar Mountain chain seems to be weaker on April 2 as the concentrations were high also over the mountainous regions in the UAE. On the third day, 3 April 2015, an overall drop of the simulated concentrations, to an overall average around 150 μg/m^3, could be noticed despite the persistence of relatively high concentrations in the southeastern region of the UAE where PM_{10} concentrations reaching 300 μg/m^3 could be reported. As shown in Fig. 8, the average PM_{10} concentration of about 150 μg/m^3 over the

Fig. 8 PM_{10} mass concentration from WRF-Chem simulations between April 1 and 3, 2015, at 10:30 local time. Simulations are from the nest domain (d02) at spatial resolution of 4 km
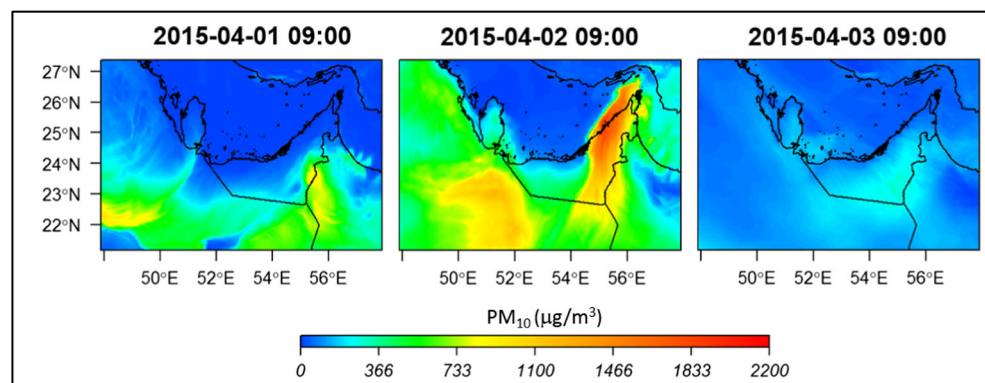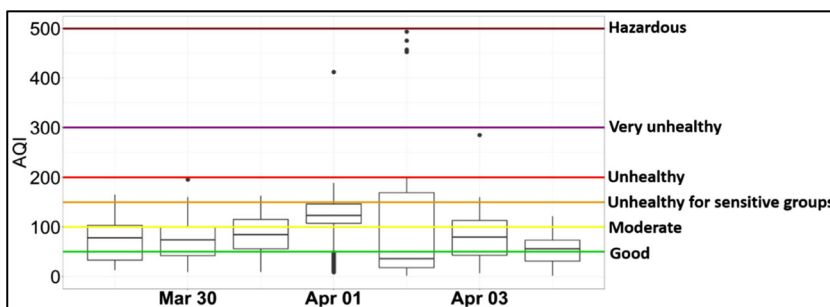
Fig. 9 Hourly distribution of Air Quality Indexes (AQIs) in the UAE during the days of the dust event from 29 March to 4 April 2015. Breakpoints for the AQIs are from the US-EPA with adjustment from the UAE air quality regulation. Data is referred to hourly AQIs calculated in the UAE over the selected period

UAE, obtained on 3 April 2015, was within the limit values allowed by the air quality regulation in the UAE (Cabinet Decree 2006). The changes in the spatial distribution of the simulated PM_{10} concentrations are in agreement with the above-inferred dynamics from the HYSPLIT back trajectories and SEVIRI imagery. On April 2, a high concentration of PM_{10} (Fig. 8) coincided with high wind speed (Fig. 4 c), as well as high intensity of AOD values (Fig. 7). In addition, the HYSPLIT back trajectories computed for 02 April showing air flow originating from southwest UAE were also corroborated by the modeled dust plume moving from Oman toward the UAE.

Spatial pattern of modeled AOD (Fig. 5 c) showed strong similarities with PM_{10} concentration (Fig. 8). This is because the model configuration that is used in the dust simulation considered dust uptakes from the soil (dust_opt = 1) as a source of particulate matter. According to this scheme, during a dust event, dust emissions are proportional to the wind speed as wind speed exceeds a threshold value. In addition, during a dust event, the effective radii of the dust particles are expected to be coarse. Therefore, both AOD and dust concentrations (PM_{10}) are computed from the aerosol extinction coefficient that is related to the dust-sized bins set in the model. Hence, pattern similarities observed between AOD and PM_{10}

Fig. 10 Breakdown of the Air Quality Indexes (AQIs) calculated in the UAE during the days of the dust event from 29 March to 4 April 2015
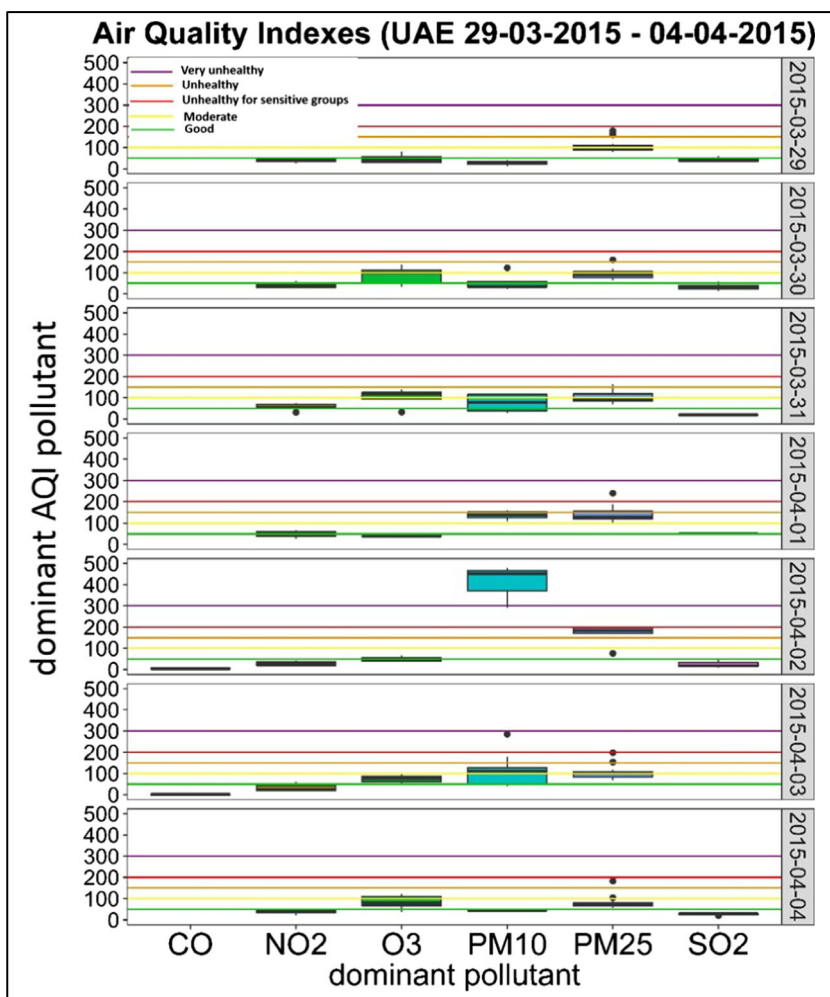
concentration might be supported by the fact that PM_{10} was mostly generated by natural contributions rather than anthropogenic contributions (Flaounas et al. 2016).

To analyze the impact of the dust event on ambient air quality conditions in the UAE, the AQI values were analyzed. The hourly distribution of the AQIs for each day during the dust event from 29 March to 4 April 2015 is shown in Fig. 9. From March 29 to 31 March, the median values of AQIs were within "good" and "moderate," indicating no threat for human health. However, on April 1 and, above all, on 2 April, AQI showed significantly high values during specific hours (Fig. 9). The highest AQIs were observed on April 2 with few isolated outlier values within the "hazardous" level of air quality. On the other hand, on April 3 and 4, the distribution of the AQIs gradually sets back within good and moderate, indicating the transitory nature of the dust event observed in the previous days.

A breakdown of the AQI analysis showed that the dominant pollutants responsible for the highest AQIs were PM_{10} and $PM_{2.5}$ (Fig. 10). More specifically, PM_{10} was the pollutant responsible for reaching the maximum AQI value during the peak time of the dust event on April 2, reaching very unhealthy levels during the dust storm in the UAE. The exceptionally high PM_{10} values even for a short time period have led to the calculation of AQI values that corresponded to hazardous conditions. A previous study that was carried out in the UAE region showed that during dust days PM_{10} is mainly composed of quartz, calcite, gypsum, and sea salt (Hamdan et al. 2016), which may suggest that such high concentrations related to hazardous conditions may have a limited adverse impact on human health. This implies that more effort should be put to establish a relationship between PM concentration and human health impact through concentration–response functions. Such relationships should account for the composition of dust in the region and the prevailing weather conditions during the events for an accurate assessment of the actual impact on public health. Recent studies carried out in Kuwait showed no evidence of any negative association between PM_{10} and all-cause of diseases during dust days (Al-Taiar and Thalib 2014; Zhang et al. 2016a). Future work will focus on expanding such analysis to the UAE. The quantification of the AQI from modeled air quality pollutants represents a novelty from this work because it might help in quantifying the impact of severe pollution events (such as dust storms) that are usually difficult to monitor with the traditional ground-based monitoring mainly because of their tendency to saturate.

Conclusions

This work investigated an extreme dust event through the integration of model, satellite, and station observation datasets. High spatial and temporal resolution satellite images, together with ground measurements from meteorological

stations, were used to assess the performance of the WRF-Chem model. The dust event, occurring over the Arabian Peninsula and moving toward the UAE from 31 March to 3 April 2015, was used as a test to assess the WRF-Chem model against satellite observations and measurements. Simulated meteorological parameters showed good agreement with observed data. The HYSPLIT model was used to track the dynamic of the dust event since its formation over the Arabian Peninsula until its transport over the UAE and dissipation through the coasts of Oman. The synoptic of the event suggested that the dust event was triggered by shamal winds that are recurrent in the region. As a result of the passage of the dense dust plume, the temperature dropped by ~ 7 °C. Strong northeast winds with speeds up to 14 m s^{-1} were observed. During the peak time of the dust storm on April 2, the highest modeled PM_{10} concentration in the UAE was about 1500 μg/m^3. Such extreme value of PM_{10} concentrations, observed during the dust storm, could be classified as a very isolated transitory episode in the UAE.

Modeling of dust over desert areas is still challenging because of lack of information about dust sinks and correct linkage with meteorology. The use of ground observations from meteorological stations and air quality stations might be used in the future to validate and correct modeled simulation of dust over the UAE as well as to understand caveats in the input data, such as emission inventory and land use data used in the WRF-Chem model. In this work, we showed that dust, mostly associated with PM_{10} particulate matter, has a significant impact on the estimation of AQIs that are commonly used to assess the degradation of air quality conditions and the impact on human health. Future work will be dedicated to the chemical characterization of dust in the UAE targeting pollution sources and the composition of the dust as well as the link with epidemiological records, which has not been, to our knowledge, addressed in the UAE and the region. This should allow for an accurate assessment of the actual impact of the recorded high AQI values on human health and determining eventually the appropriate local air quality standards.

Finally, this work represents a first attempt to use the WRF-Chem results to estimate AQI over the UAE as well as the possibility to use two satellite products (MODIS-MAIAC and MSG-SEVIRI) to track dust over the UAE. The high spatial resolution of the satellite data improved the validation and comparison with ground-based and modeled data. In addition, in this work, we were able to quantify the level of agreement and accuracy from the comparison between ground observations and modeled data for meteorological parameters and aerosols. We could conclude that the use of an air quality model over the UAE, such as the WRF-Chem, could represent an added value to quantify Air Quality Indexes during severe dust events that would otherwise be very difficult to detect with the traditional monitoring systems. Finally, this work showed the added value of using high spatial resolution

satellite data as future datasets that could be assimilated in air quality modeling to increase accuracy when forecasting air quality conditions.

Publisher's note Springer Nature remains neutral with regard to jurisdictional claims in published maps and institutional affiliations.

References

Ackerman SA, Chung H (1992) Radiative effects of airborne dust on regional energy budgets at the top of the atmosphere. J Appl Meteor 31:223–233. https://doi.org/10.1175/1520-0450(1992)031<0223:REOADO>2.0.CO;2

Ackermann IJ, Hass H, Memmesheimer M, Ebel A, Binkowski FS, Shankar U (1998) Modal aerosol dynamics model for Europe: development and first applications. Atmos Environ 32:2981–2999. https://doi.org/10.1016/S1352-2310(98)00006-5

Al Azhar M, Temimi M, Zhao J, Ghedira H (2016) Modeling of circulation in the Arabian Gulf and the Sea of Oman: skill assessment and seasonal thermohaline structure. J Geophys Res Oceans 121:1700–1720. https://doi.org/10.1002/2015JC011038

Aldababseh A, Temimi M (2017) Analysis of the variability of poor visibility events in north and central United Arab Emirates. AGU Fall Meet Abstr 23:A23E-0266

Al-Taiar A, Thalib L (2014) Short-term effect of dust storms on the risk of mortality due to respiratory, cardiovascular and all-causes in Kuwait. Int J Biometeorol 58:69–77. https://doi.org/10.1007/s00484-012-0626-7

Banks JR, Brindley HE (2013) Evaluation of MSG-SEVIRI mineral dust retrieval products over North Africa and the Middle East. Remote Sens Environ 128:58–73. https://doi.org/10.1016/j.rse.2012.07.017

Barkley MP, González Abad G, Kurosu TP, Spurr R, Torbatian S, Lerot C (2017) OMI air-quality monitoring over the Middle East. Atmos Chem Phys 17:4687–4709

Basha G, Phanikumar DV, Kumar KN, Ouarda TBMJ, Marpu PR (2015) Investigation of aerosol optical, physical, and radiative characteristics of a severe dust storm observed over UAE. Remote Sensing of Environment 169:404–417. https://doi.org/10.1016/j.rse.2015.08.033

Beegum SN, Gherboudj I, Chaouch N, Temimi M, Ghedira H (2018) Simulation and analysis of synoptic scale dust storms over the Arabian Peninsula. Atmos Res 199:62–81. https://doi.org/10.1016/j.atmosres.2017.09.003

Cautenet G, Legrand M, Cautenet S, Bonnel B, Brogniez G (1992) Thermal impact of Saharan dust over land. Part I: simulation. J Appl Meteor 31:166–180. https://doi.org/10.1175/1520-0450(1992)031<0166:TIOSDO>2.0.CO;2

Chaouch N, Temimi M, Weston M, Ghedira H (2017) Sensitivity of the meteorological model WRF-ARW to planetary boundary layer schemes during fog conditions in a coastal arid region. Atmos Res 187:106–127. https://doi.org/10.1016/j.atmosres.2016.12.009

Chen F, Dudhia J (2001) Coupling an advanced land surface– hydrology model with the Penn State–NCAR MM5 modeling system. Part I: Model implementation and sensitivity. Mon Wea Rev 129:569–585

Cheng WYY, Carrió GG, Cotton WR, Saleeby SM (2009) Influence of cloud condensation and giant cloud condensation nuclei on the development of precipitating trade wind cumuli in a large eddy simulation. J Geophys Res Atmos 114. https://doi.org/10.1029/2008JD011011

Chou M, Suarez M (1994) An efficient thermal infrared radiation parameterization for use in general circulation models. NASA Tech. Memo. 104606, 85pp. [Available from NASA Center for Aerospace Information, 800 Elkridge Landing Road, Linthicum Heights, MD 21090–2934]

Cremades PG, Fernández RP, Allende DG, Mulena GC, Puliafito SE (2017) High resolution satellite derived erodibility factors for WRF/Chem windblown dust simulations in Argentina. Atmósfera 11–25. https://doi.org/10.20937/ATM.2017.30.01.02

Crook J (2009) Climate analysis and long range forecasting of dust storms in Iraq Master's thesis, Naval Postgraduate School,Monterey, CA

Decree UC (2006) Regulation Concerning Protection of Air from Pollution in the UAE. https://www.ead.ae/Documents/PDF-Files/Federal-Bylaw-12-Air-pollution-2006-English-translation.pdf. Accessed 28 Jan 2019.

ElTahan M, Shokr M, Sherif AO (2017) Tuning dust schemes in weather research forecast for simulating severe events over Egypt. In: EGU General Assembly Conference Abstracts, 2017/04/01/ 2017. p 6115

EPA U (2006) EPA QA/G-9R, February 2006, Data quality assessment: A reviewer's guide

Flaounas E, Kotroni V, Lagouvardos K, Klose M, Flamant C, Giannaros TM (2016) Assessing atmospheric dust modelling performance of WRF-Chem over the semi-arid and arid regions around the Mediterranean. Atmos Chem Phys Discuss 2016:1–28. https://doi.org/10.5194/acp-2016-307

Furman HKH (2003) Dust storms in the Middle East: sources of origin and their temporal characteristics. Indoor Built Environ 12:419–426. https://doi.org/10.1177/1420326X03037110

Ghebreyesus DT, Temimi M, Fares A, Bayabil HK (2016) A multi-satellite approach for water storage monitoring in an arid watershed. Geosciences 6:33. https://doi.org/10.3390/geosciences6030033

Giannakopoulou EM, Toumi R (2012) The Persian Gulf summertime low-level jet over sloping terrain. QJR Meteorol Soc 138:145–157. https://doi.org/10.1002/qj.901

Ginoux P, Chin M, Tegen I, Prospero JM, Holben B, Dubovik O, Lin S-J (2001) Sources and distributions of dust aerosols simulated with the GOCART model. J Geophys Res 106(D17):20255–20273. https://doi.org/10.1029/2000JD000053

Goudie AS, Middleton NJ (2006) Desert dust in the global system. Springer, Heidelberg

Greet J-M et al (2012) EDGAR-HTAP: a harmonized gridded air pollution emission dataset based on national inventories. European Commission, Joint Research Centre, Institute for Environment and Sustainability, JRC Scientific and Technical Reports, Luxembourg

Grell GA, Peckham SE, Schmitz R, McKeen SA, Frost G, Skamarock WC, Eder B (2005) Fully coupled "online" chemistry within the WRF model. Atmos Environ 39:6957–6975. https://doi.org/10.1016/j.atmosenv.2005.04.027

Hamdan NM, Alawadhi H, Jisrawi N (2016) Particulate matter pollution in the United Arab Emirates: elemental analysis and phase identification of fine particulate pollutants ICEPR 158, Proceedings of the 2nd World Congress on New Technologies (NewTech'16) doi: 10.11159/icepr16.158

Hamidi M, Kavianpour MR, Shao Y (2013) Synoptic analysis of dust storms in the Middle East Asia-Pacific. J Atmos Sci 49:279–286. https://doi.org/10.1007/s13143-013-0027-9

Haywood J, Boucher O (2000) Estimates of the direct and indirect radiative forcing due to tropospheric aerosols: a review. Rev Geophys 38:513–543. https://doi.org/10.1029/1999RG000078

Holben BN, Eck TF, Slutsker I, Tanré D, Buis JP, Setzer A, Vermote E, Reagan JA, Kaufman YJ, Nakajima T, Lavenu F, Jankowiak I, Smirnov A (1998) AERONET—a federated instrument network and data archive for aerosol characterization. Remote Sens Environ 66:1–16. https://doi.org/10.1016/S0034-4257(98)00031-5

Hong S, Noh Y, Dudhia J (2006) A New Vertical Diffusion Package with an Explicit Treatment of Entrainment Processes. Mon Wea Rev 134:2318–2341, https://doi.org/10.1175/MWR3199.1

Hsu NC et al (2013) Enhanced Deep Blue aerosol retrieval algorithm: the second generation. J Geophys Res Atmos 118:9296–9315. https://doi.org/10.1002/jgrd.50712

Jish Prakash P, Stenchikov G, Kalenderski S, Osipov S, Bangalath H (2015) The impact of dust storms on the Arabian Peninsula and the Red Sea. Atmos Chem Phys 15:199–222. https://doi.org/10.5194/acp-15-199-2015

Kalnay E et al (1996) The NCEP/NCAR 40-year reanalysis project. Bull Amer Meteor Soc 77:437–472. https://doi.org/10.1175/1520-0477(1996)077<0437:tnyrp>2.0.co;2

Kim H-S, Chung Y-S (2008) Satellite and ground observations for large-scale air pollution transport in Yellow Sea region. J Atmos Chem 60:103–116. https://doi.org/10.1007/s10874-008-9111-4

Kim H-S, Chung Y-S, Lee S-G (2012) Characteristics of aerosol types during large-scale transport of air pollution over the Yellow Sea region and at Cheongwon, Korea, in 2008. Environ Monit Assess 184:1973–1984. https://doi.org/10.1007/s10661-011-2092-9

Kim H-S, Chung Y-S, Yoon M-B (2016) An analysis on the impact of large-scale transports of dust pollution on air quality in East Asia as observed in Central Korea in 2014. Air Qual Atmos Health 9:83–93. https://doi.org/10.1007/s11869-014-0312-5

Lin Y-L, Farley RD, Orville HD (1983) Bulk parameterization of the snow field in a cloud model. J Clim Appl Meteorol 22:1065–1092

Liu J, Zheng Y, Li Z, Cribb M (2011) Analysis of cloud condensation nuclei properties at a polluted site in southeastern China during the AMF-China Campaign. J Geophys Res Atmos 116:116. https://doi.org/10.1029/2011JD016395

Lyapustin A, Wang Y, Korkin S, Huang D (2018) MODIS collection 6 MAIAC algorithm. Atmos Meas Tech 11:5741–5765. https://doi.org/10.5194/amt-11-5741-2018

Mailler S et al (2017) CHIMERE-2017: from urban to hemispheric chemistry-transport modeling. Geosci Model Dev 10:2397–2423. https://doi.org/10.5194/gmd-10-2397-2017

Markowicz KM, Flatau PJ, Vogelmann AM, Quinn PK, Welton EJ (2003) Clear-sky infrared aerosol radiative forcing at the surface and the top of the atmosphere. QJR Meteorol Soc 129:2927–2947. https://doi.org/10.1256/qj.02.224

MétéoFrance (2011) Algorithm theoretical basis document for cloud products (CMa-PGE01 v3.2, CT-PGE02 v2.2 & CTTH-PGE03 v2.2). Technical Report SAF/NWC/CDOP/MFL/ SCI/ATBD/01. MétéoFrance, Paris

Mezhoud N, Temimi M, Zhao J, Al Shehhi MR, Ghedira H (2016) Analysis of the spatio-temporal variability of seawater quality in the southeastern Arabian Gulf. Mar Pollut Bull 106:127–138. https://doi.org/10.1016/j.marpolbul.2016.03.016

Michael Reynolds R (1993) Physical oceanography of the Gulf, Strait of Hormuz, and the Gulf of Oman—results from the Mt Mitchell expedition. Mar Pollut Bull 27:35–59. https://doi.org/10.1016/0025-326X(93)90007-7

Middleton N (1986) Dust storms in the Middle East. J Arid Environ 10:10–96. https://doi.org/10.1016/S0140-1963(18)31249-7

Miller D et al (2008) Haboob dust storms of the southern Arabian Peninsula. J Geophys Res-Atmos 113:113. https://doi.org/10.1029/2007JD008550

Mlawer EJ, Taubman SJ, Brown PD, Iacono MJ, Clough SA (1997) Radiative transfer for inhomogeneous atmospheres: RRTM, a validated correlated-k model for the longwave. J Geophys Res Atmos 102:16663–16682. https://doi.org/10.1029/97JD00237

Monin AS, Obukhov AM (1954) Basic laws of turulent mixing in the atmosphere near the ground. Tr Inst Teor Geofiz Akad Nauk SSSR 24:1963–1987.

Nabavi SO, Haimberger L, Samimi C (2017) Sensitivity of WRF-chem predictions to dust source function specification in West Asia. Aeolian Res 24:115–131. https://doi.org/10.1016/j.aeolia.2016.12.005

NCM (2011) Dust sources affecting the United Arab Emirates, report. Abu Dhabi

Notaro M, Alkolibi F, Fadda E, Bakhrjy F (2013) Trajectory analysis of Saudi Arabian dust storms. J Geophys Res (Atmos) 118:6028–6043. https://doi.org/10.1002/jgrd.50346

Ouarda TBMJ, Charron C, Niranjan Kumar K, Marpu PR, Ghedira H, Molini A, Khayal I (2014) Evolution of the rainfall regime in the United Arab Emirates. J Hydrol 514:258–270. https://doi.org/10.1016/j.jhydrol.2014.04.032

Peckham SE, Smirnova TG, Benjamin SG, Brown JM, Kenyon JS (2015) Implementation of a digital filter initialization in the WRF model and its application in the Rapid Refresh. Mon Wea Rev 144:99–106. https://doi.org/10.1175/MWR-D-15-0219.1

Perrone TJ (1979) Winter shamal in the Persian Gulf, Nav Environ Predict Res Facility, Technical Report, Monterey. pp 180

Prospero JM, Ginoux P, Torres O, Nicholson SE, Gill TE (2002) Environmental characterization of global sources of atmospheric soil dust identified with the Nimbus 7 Total Ozone Mapping Spectrometer (TOMS) absorbing aerosol product. Rev Geophys 40:1002. https://doi.org/10.1029/2000RG000095

Radi A, Awad A, Dhanhani A (2008) Implementation and preliminary tests of an air quality forecasting system based on WRF-Chem over Middle-East, Arabian Peninsula and United Arab Emirates

Rizza U et al (2018) Sensitivity of WRF-Chem model to land surface schemes: assessment in a severe dust outbreak episode in the Central Mediterranean (Apulia region). Atmos Res 201:168–180. https://doi.org/10.1016/j.atmosres.2017.10.022

Schell B, Ackermann IJ, Hass H, Binkowski FS, Ebel A (2001) Modeling the formation of secondary organic aerosol within a comprehensive air quality model system. J Geophys Res Atmos 106:28275–28293. https://doi.org/10.1029/2001JD000384

Schmetz J, Pili P, Tjemkes S, Just D, Kerkmann J, Rota S, Ratier A (2002) An introduction to Meteosat Second Generation (MSG). Bull Amer Meteor Soc 83:977–992. https://doi.org/10.1175/1520-0477(2002)083<0977:AITMSG>2.3.CO;2

Seinfeld JH et al (2016) Improving our fundamental understanding of the role of aerosol−cloud interactions in the climate system. PNAS 113:5781–5790. https://doi.org/10.1073/pnas.1514043113

Shao Y et al (2011) Dust cycle: an emerging core theme in earth system science. Aeolian Res 2:181–204. https://doi.org/10.1016/j.aeolia.2011.02.001

Shell KM, Somerville RCJ (2007) Direct radiative effect of mineral dust and volcanic aerosols in a simple aerosol climate model, J Geophys Res 112:D03206. https://doi.org/10.1029/2006JD007198

Stein AF, Draxler RR, Rolph GD, Stunder BJB, Cohen MD, Ngan F (2015) NOAA's HYSPLIT atmospheric transport and dispersion modeling system. Bull Amer Meteor Soc 96:2059–2077. https://doi.org/10.1175/BAMS-D-14-00110.1

Tegen I, Lacis AA (1996) Modelling of particle size distribution and its influence on the radiative properties of mineral dust aerosol. J Geophys Res 101(D14):19237–19244. https://doi.org/10.1029/95JD03610

Wehbe Y, Ghebreyesus D, Temimi M, Milewski A, Al Mandous A (2017) Assessment of the consistency among global precipitation products over the United Arab Emirates. J Hydrol Reg Stud 12:122–135. https://doi.org/10.1016/j.ejrh.2017.05.002

Wehbe Y, Temimi M, Ghebreyesus DT, Milewski A, Norouzi H, Ibrahim E (2018) Consistency of precipitation products over the Arabian Peninsula and interactions with soil moisture and water storage AU - Wehbe, Youssef. Hydrol Sci J 63:408–425. https://doi.org/10.1080/02626667.2018.1431647

Weston M, Chaouch N, Valappil V, Temimi M, Ek M, Zheng W (2018) Assessment of the sensitivity to the thermal roughness length in Noah and Noah-MP land surface model using WRF in an arid region. Pure Appl Geophys. https://doi.org/10.1007/s00024-018-1901-2

Wilkerson WD (1991) Dust and sand forecasting in Iraq and adjoining countries Tech Note AWS/TN-91/001, Air Weather Serv, Scott AFB, III:63 pp

Yousef LA, Temimi M, Wehbe Y, Al Mandous A (2019) Total cloud cover climatology over the United Arab Emirates. Atmos Sci Lett. 20:e883. https://doi.org/10.1002/asl.883

Zhang T, Gong W, Zhu Z, Sun K, Huang Y, Ji Y (2016a) Semi-physical estimates of national-scale PM10 concentrations in China using a satellite-based geographically weighted regression model. Atmosphere 7:88. https://doi.org/10.3390/atmos7070088

Zhang X, Zhao L, Tong D, Wu G, Dan M, Teng B (2016b) A systematic review of global desert dust and associated human health effects. Atmosphere 7:158. https://doi.org/10.3390/atmos7120158